Fatigue crack growth in the cruciform specimens under out-of-phase loading

Dariusz Rozumek, Cyprian T. Lachowicz & Ewald Macha[1]

[1] Opole University of Technology, ul. Mikołajczyka 5, 45-271 Opole, Poland
e-mail: d.rozumek@po.opole.pl

ABSTRACT. *The paper presents the experimental results concerning fatigue crack growth in the cruciform plate specimens made of 18G2A (S355J0) steel. Two variants of specimens were used, one with stress concentrator in form of central hole of 3.0 mm (with the minimum 1.86 mm wall thickness) in diameter and other without a hole (the minimum 1.25 mm wall thickness). The analytic and numerical methods was applied for description of fatigue crack growth rate. Simulation of crack growth in cruciform specimens were performed with the finite element method and the COMSOL software (up to the crack initiation), as well as with the boundary element method and the FRANC3D software (during propagation).*

INTRODUCTION

Investigations on initiation and growth of fatigue cracks in cruciform specimens are rarely performed because they require special test stands. The paper [1] presents the tests of plexiglass cruciform specimens with the initiated slots at the angles 45° and 90° to the horizontal axis. The stress intensity factors for modes I and II were calculated with the boundary element method. The authors of [2] tested cruciform specimens and two steels (cyclically hardened and cyclically softened). The tests included strain control and measurements of the fatigue crack lengths. Initiation and growth of corner fatigue cracks (shapes of ¼ of the circle and ¼ of the ellipse in the specimen section) are described in [3]. The tests were performed at the biaxial fatigue test stand. Plane cruciform specimens were tested under two loading ratios: $P_x : P_y = 1 : 1$ and $1 : 0.5$. Calculations were carried out with the finite element method, too. The paper [4] presents the fatigue crack growth tests in plane cruciform specimens made of steel with central holes, and solid specimens subjected to tension-compression. Intense development of numerical methods causes that they are more and more often applied, and they even supplant analytical methods. Numerical methods allow to calculate strains and stresses near the crack tip, or crack tip opening displacements - their experimental measurement is difficult or even impossible, and analytical methods are not efficient, or they cannot be applied. However, using numerical method we must verify the obtained results. In some papers we can find the calculated results obtained by numerical methods, without relation to any real data.

The aim of this paper is to compare the experimental results of fatigue crack growth rate from tests of cruciform specimens made of 18G2A steel with calculated results obtained by means of numerical and analytical methods.

EXPERIMENTS

Plane cruciform specimens were tested. Fig. 1 shows a scheme of specimen with the central hole. The specimens were made of low-alloy higher-strength steel 18G2A (S355J0) included in the standard PN-EN 10025 of 2002. Steel S355J0 is widely applied for elements of supporting structures, such as bridges, cranes, overhead cranes, big diameter high-pressure pipelines etc. Some mechanical properties of the tested steel are given in Table 1.

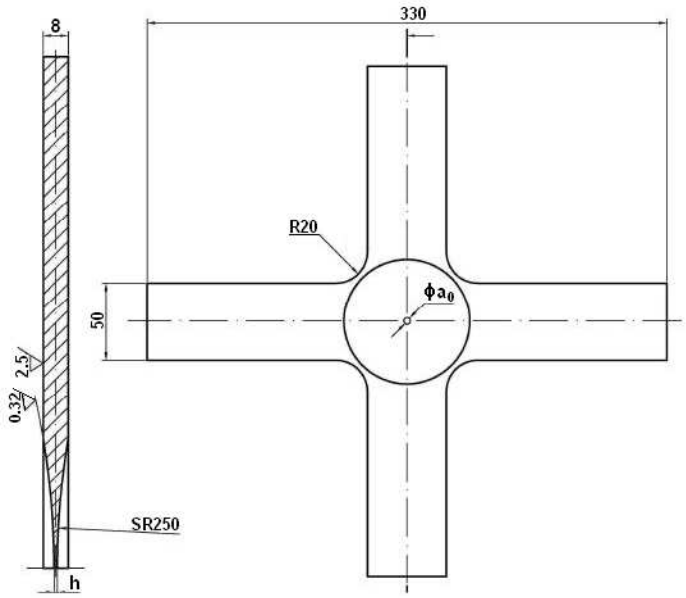

Figure 1. Specimen for tests of fatigue crack growth, dimensions in mm

Table 1. Mechanical properties of 18G2A steel

Yield stress σ_{YS} (MPa)	Ultimate stress σ_U (MPa)	Elastic modulus E (GPa)	Poisson`s ratio ν
357	535	210	0.30

The central part of the specimen, having spherical contour (SR250), was obtained by precise turning. Next, the central surface was polished with abrasive paper of decreasing granularity. In the central part of the spherical surface (with the minimum wall thickness h = 1.86 mm) a hole of diameter a_0 = 3.0 mm was made. The theoretical stress

concentration factor in the specimen K_t = 2.84, was estimated with use of the model in paper [5]. In the solid specimen (without a hole) the minimum wall thickness was h = 1.25 mm. Coefficients of the cyclic strain curve under tension-compression in the Ramberg-Osgood equation for 18G2A steel are the following [4]: the cyclic strength coefficient K′ = 1323 MPa, the cyclic strain hardening exponent n′ = 0.207. The test results presented in this paper were obtained at Opole University of Technology, in Department of Mechanics and Machine Design [6]. The tests were performed at the fatigue test stand MZPK 100 (Fig. 2) which allowed to realize cyclically and randomly variable histories under static mean value of loading. The tests were performed under loading with the controlled force (P_x, P_y), and constant positions of the intersection points of force directions in axes x, y were kept. Sinusoidal loadings were applied to the specimen arms, they had the same frequencies f = 13 Hz and similar amplitudes of forces $P_{x,a}$ and $P_{y,a}$ with phase shift by 180^o (coefficient of cross-correlation between force courses P_x (t), P_y (t), shown in Fig. 3 was r = - 1). Loadings of the specimens with holes were: $P_{x,a1\text{-}3}$ = 13.55 kN and $P_{y,a2\text{-}4}$ = 13.30 kN, which corresponded to the nominal amplitude of normal stress $\sigma_{a,1\text{-}3}$ = 105 MPa ($\sigma_{max} = K_t\sigma_a$ = 298 MPa) and $\sigma_{a,2\text{-}4}$ = 103 MPa ($\sigma_{max} = K_t\sigma_a$ = 293 MPa) before the crack initiation. Loadings of the specimens without the holes were: $P_{x,a1\text{-}3}$ = 21.80 kN i $P_{y,a2\text{-}4}$ = 21.50 kN, which corresponded to the nominal amplitude of normal stress $\sigma_{a,1\text{-}3}$ = 209 MPa and $\sigma_{a,2\text{-}4}$ = 206 MPa before the crack initiation. Fatigue tests were performed in the high cycle fatigue regime (HCF) under the stress ratio R = - 1.

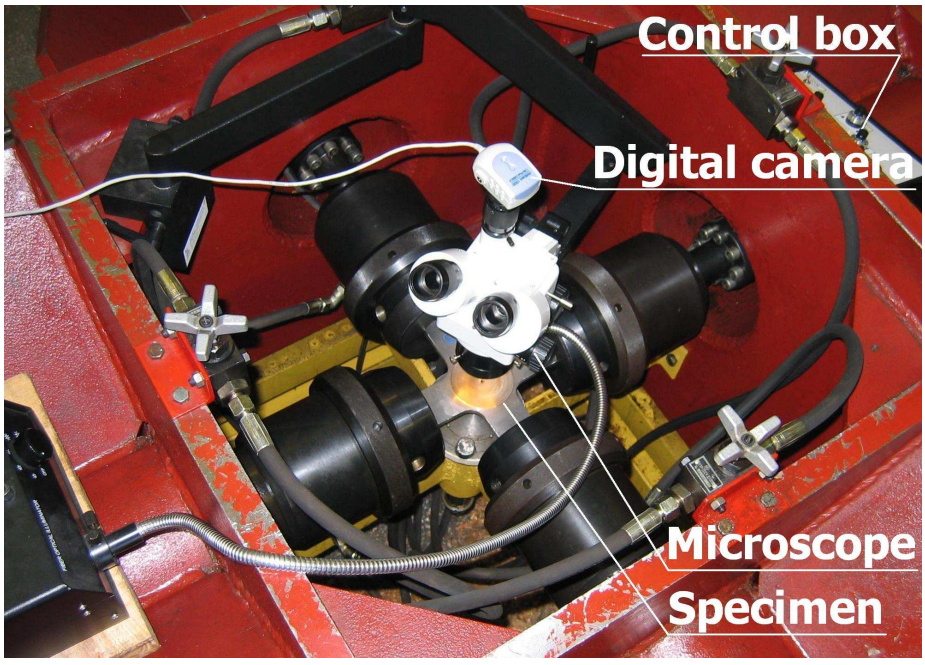

Figure 2. The MZPK-100 fatigue stand setup with portable microscope

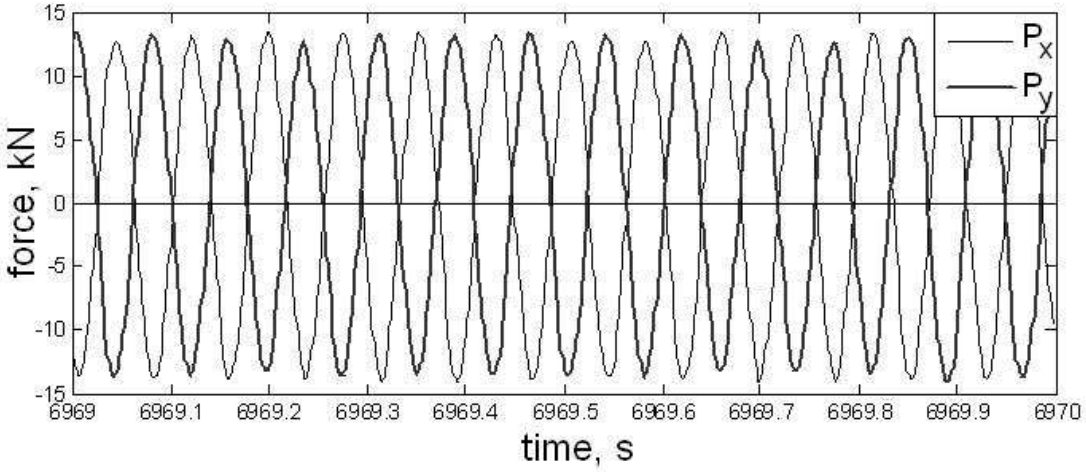

Figure 3. Fragment of force courses $P_x(t)$, $P_y(t)$ with the cross-correlation coefficient r = - 1

Pictures of one surface of the specimen with fatigue cracks were cyclically registered with the optical microscope (magnification 7x) and the digital camera (0.0085 mm/pixel). The pictures were used for measurements of the fatigue crack lengths "a". While performing tests, also the number of loading cycles N was registered. Strains were measured with strain gauge rosettes of the measuring base 1 mm.

THE TEST RESULTS AND THEIR ANALYSIS

The fatigue crack lengths were measured and the number of cycles to the crack initiation N_i, i.e. to occurrence of an apparent crack of length $a_i = 0.07 \div 0.20$ mm, was determined. In the specimens with holes and the solid specimens usually four cracks for mode I could be seen (see Fig. 4). In one case, three cracks were observed in the specimen with the central hole. The cracks shown were in specimens loaded by similar force amplitudes, but the maximum stresses near the cracks a_1 and a_3 were shift in phase by 180^o related to the stresses near a_2 and a_4. In the specimen with a hole shown in Fig. 4a the cracks developed for mode I. In the solid specimen shown in Fig. 4b the cracks developed for mixed mode I + II (for short cracks of lengths to a = 0.56 mm at the angle about 31° to the y axis). Then, the cracks developed for mode I. In the same specimen and under the same loading, particular cracks initiated under different numbers of cycles N_i (Fig. 5). A characteristic feature of the observed cracks, independent of loading level, was stabilization of the crack growth rate for specimens with holes at the length $a \geq 1$ mm (Fig. 5a), and for solid specimens – at the length $a \geq 3$ mm (Fig. 5b). Comparing the test results shown in Fig. 5 (symbols are used, ◇ - a_1, △ - a_2, □ - a_3, ∇- a_4) for the curves a = f (N), we can notice different shapes of the curves at the initial stage of crack growth. In the case of the specimens with holes, the shape of the curve is similar to

logarithmic curves, and for the solid specimens (without a hole) the test results form a shape of exponential curves.

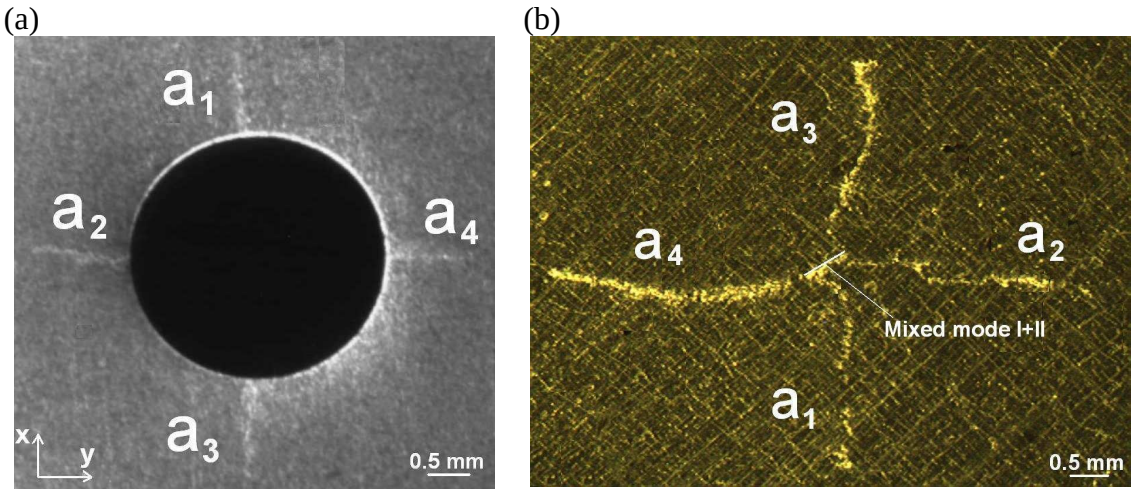

Figure 4. Crack growth in specimens (a) with a hole, (b) without a hole

Fig. 5 contains values of the fatigue crack growth rate determined with the use of linear regression with the least square method for crack lengths greater than 1 mm (specimen with the hole) and greater than 5 mm (solid specimen). In all the cases, the coefficients of correlation are r = 0.995 ÷ 0.999, and the crack growth rates da/dN have similar values for the considered specimens (see Fig. 5).

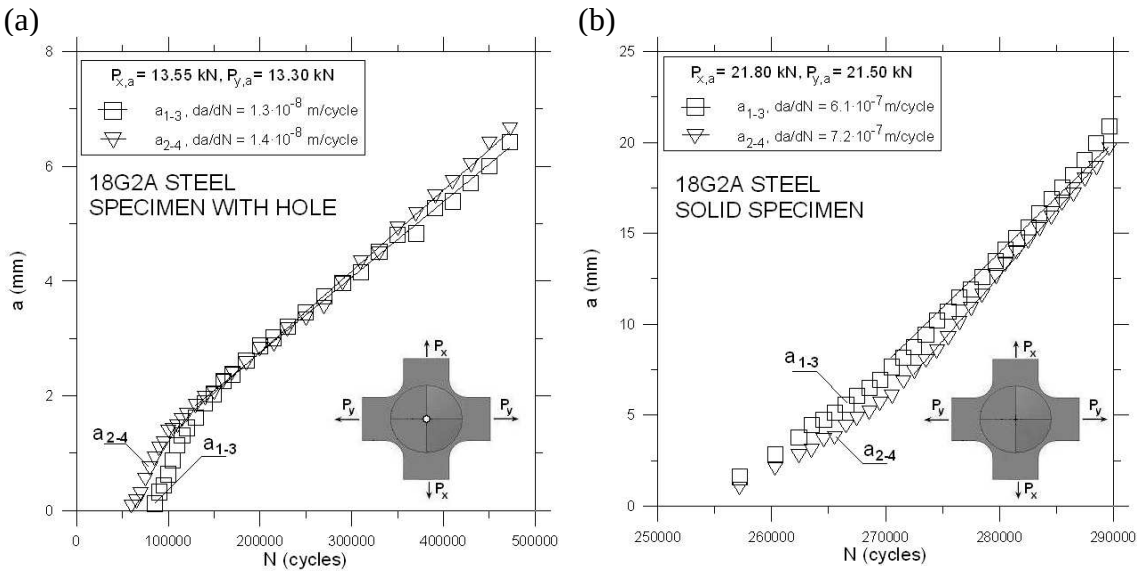

Figure 5. Dependencies of fatigue crack length versus number of cycles N for specimens: (a) with a hole, (b) without a hole

The analytic approximate method was applied for description of fatigue crack growth rate because of a complicated shape of the specimen, and in calculations the cruciform specimen (biaxially loaded) was replaced by two plane specimens uniaxially loaded along x and y axes. While tests, when the x axis was subjected to tension, the y axis was subjected to compression and inversely (Fig. 3). Moreover, numerical calculations of stresses, strains and stress intensity factors (SIF`s) were performed with the finite element method and the COMSOL software [7] (up to the crack initiation), as well as with the boundary element method (BEM) and the FRANC3D software [8] (during propagation). Fig. 6 shows the distribution of the maximum principal stresses for 1/8 geometry of the specimen with a hole [6], and distribution of the stresses σ_{xx} along the line y shown in the figure (COMSOL software). From Fig. 6 it appears that the stresses σ_{xx} stabilize about 2.5 mm from the hole edge.

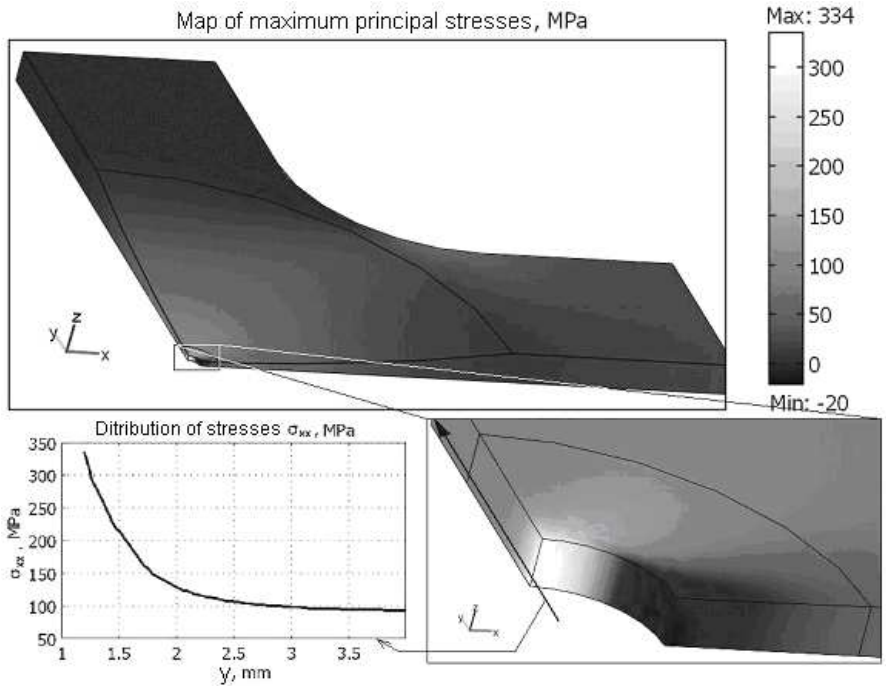

Figure 6. Distribution of the maximum principal stresses for 1/8 geometry of the specimen with a hole, and distribution of the stresses σ_{xx} along the line y shown in the figure [6]

Simulation of crack growth in cruciform specimens was performed with use of the FRANC3D software. The geometrical model of the specimen was created using OSM software, and the boundary element mesh was generated in the FRANC3D software. The BES software was applied for calculations. The authors decided to perform linear-elastic analysis. The boundary element mesh was software generated and it contained more than 3814 triangular and quadrangular elements. The observed crack growth was

divided into 15 steps, and next they were realized in the FRANC3D and BES software. The crack growth direction was assumed on the basis of observation of the actual crack path obtained from tests. Such simulation of the crack propagation allows to obtain the stress maps for each realized crack increment. In the calculated model, cracks were initiated at the hole edge as through cracks of the initial length 0.07 mm. The initial minimum number of boundary (finite) elements along the crack length was twelve. Figs. 7, 8 present a mesh of boundary elements for all the models of the specimen with a hole and solid specimen and the magnified central area of the models together with the cracks.

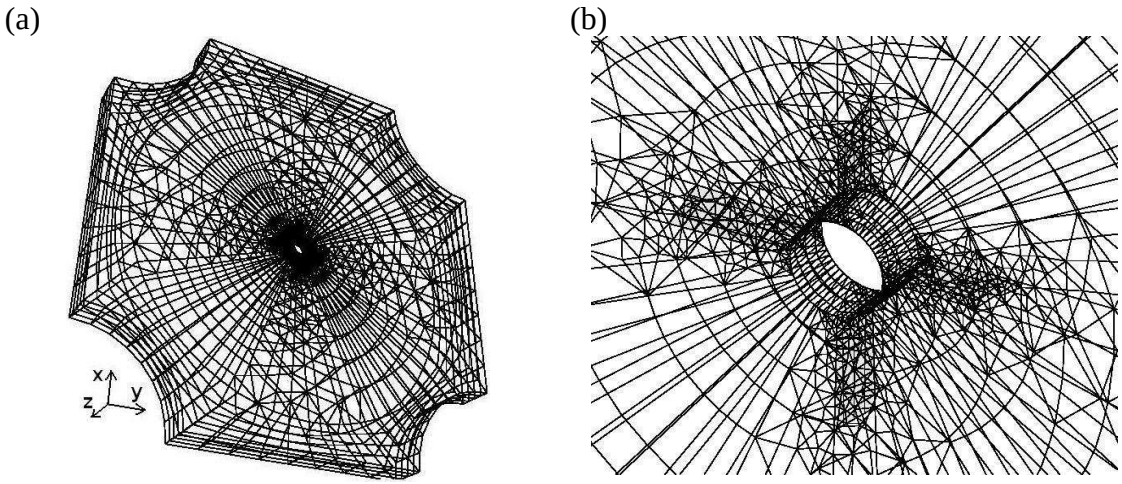

Figure 7. Mesh of the boundary elements for the specimen with a hole: (a) all the surface, (b) magnified central area

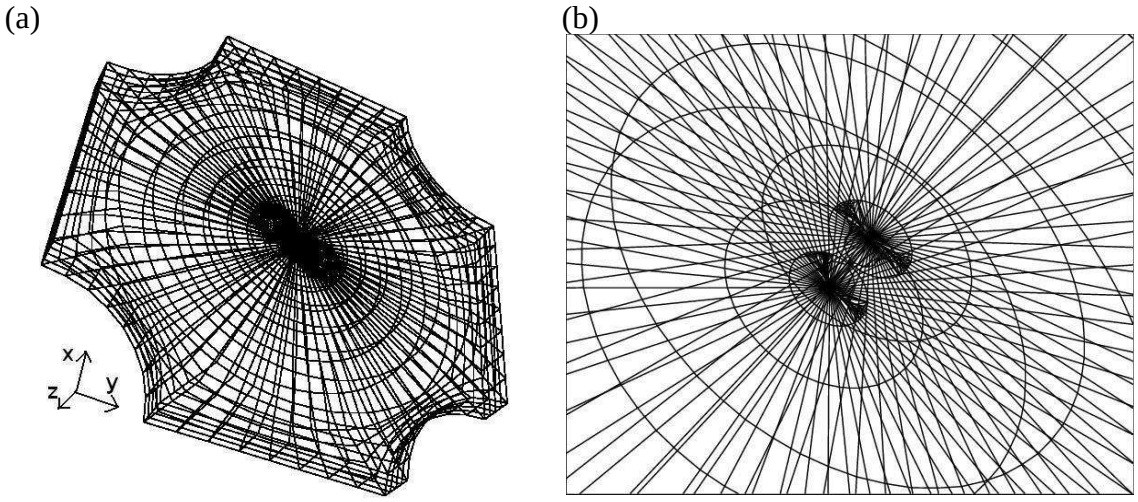

Figure 8. Mesh of boundary elements for the solid specimen: (a) all the surface, (b) magnified central area

The biggest concentration of the mesh can be seen in the crack growth area. Some exemplary results of numerical calculations obtained with the FRANC3D and BES software for tension-compression and the specimen with the central hole and the specimen without the hole made of 18G2A steel are shown in Figs. 9 and 10 as the stress maps (the scale with the corresponding stresses is shown near the figures).
Fig. 9a shows the stresses σ_{xx} formed in the specimen model under tension along x-axis (compression along y-axis) for the applied loading $P_{x,a}$ = 13.55 kN, and the crack length a = 6.65 mm. In Fig. 9b one can see the stresses σ_{yy} formed in the specimen model under tension along y-axis (compression under x-axis) for the applied loading $P_{y,a}$ = 13.30 kN, and the crack length a = 6.42 mm.

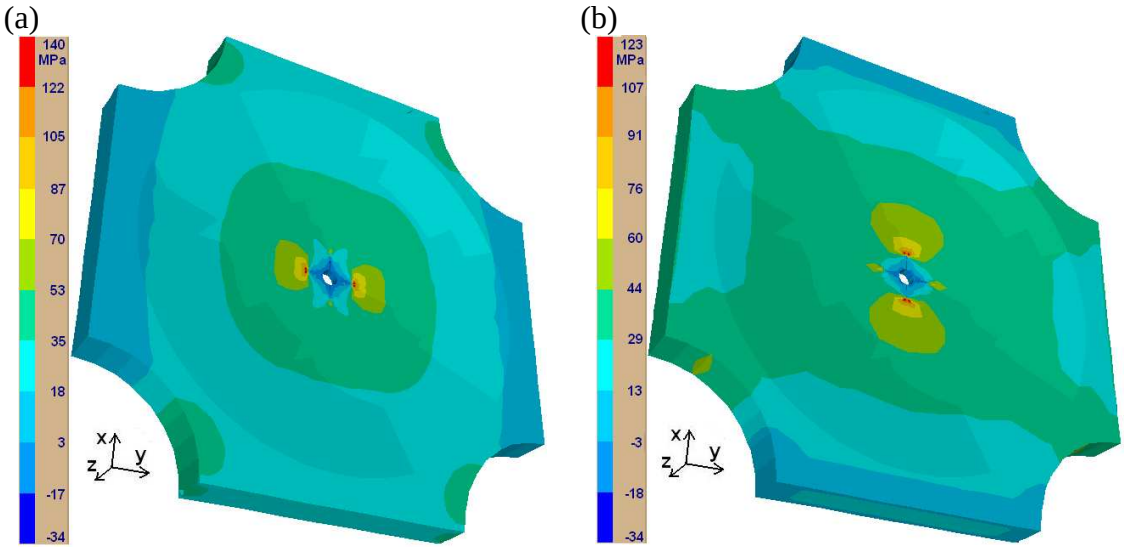

Figure 9. The components σ_{xx} and σ_{yy} of the stress tensor under tension-compression of the specimen with a hole for the crack length a = 6.65 mm: (a) $P_{x,a}$ = 13.55 kN, (b) $P_{y,a}$ = 13.30 kN

Fig. 10a shows the stresses σ_{xx} formed in the specimen model under tension along x-axis (compression along y-axis) for the applied loading $P_{x,a}$ = 21.80 kN, and the crack length a = 0.56 mm. Fig. 10b presents the stresses σ_{yy} formed in the specimen model under tension along y-axis (compression along x-axis) for the applied loading $P_{y,a}$ = 21.50 kN, and the crack length a = 0.56 mm. Characteristics of the fatigue crack growth rates da/dN versus the range of stress intensity factor ΔK for loadings along with axes x and y respectively are presented in Fig. 11. In Fig. 11a we can see increase of crack growth rate from da/dN = $4.0 \cdot 10^{-8}$ m/cycle to da/dN = $5.8 \cdot 10^{-8}$ m/cycle, which corresponds to the initial constant thickness of the specimen h = 1.86 mm. Next, we observe decrease of the crack growth rate to about da/dN = $1.8 \cdot 10^{-8}$ m/cycle and its stabilization within da/dN = $1.8 \cdot 10^{-8} \div 1.0 \cdot 10^{-8}$ m/cycle.

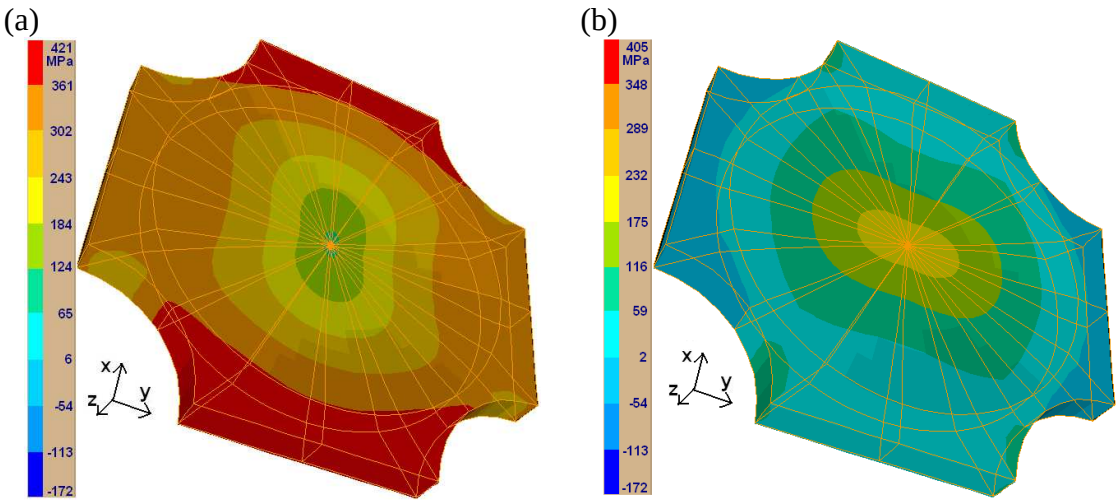

Figure 10. The components σ_{xx} and σ_{yy} of the stress tensor under tension-compression of the solid specimen for the crack length a = 0.56 mm: (a) $P_{x,a}$ = 21.80 kN, (b) $P_{y,a}$ = 21.50 kN

Such behaviour of cracks can be explained by increase of the specimen thickness which stabilizes the crack growth rate. Similar behaviour could be observed in the case of all tested specimens with holes.

In the solid specimen (Fig. 11b), typical behaviour of cracks (progressive increase of cracking) was observed in both x and y axes. The experimental results shown in Fig. 11 of crack growth rate as a function of the stress intensity factor range were described with the Paris equation [9]

$$\frac{da}{dN} = C(\Delta K)^m, \tag{1}$$

where $\Delta K = K_{max} - K_{min}$.

For the specimens with the holes the range of the stress intensity factor for mode I is calculated from

$$\Delta K = Y_1 \Delta\sigma_{nom} \sqrt{\pi(a + a_0)}, \tag{2}$$

and for the solid specimens we use the following equation

$$\Delta K = Y_2 \Delta\sigma_{nom} \sqrt{\pi a}, \tag{3}$$

where $\Delta\sigma_{nom}$ is the stress range under tension and compression ($\Delta\sigma_{nom} = 2\sigma_a$, $\sigma_a = P_a/S$, rectangular cross-section S = wh, w = 50 mm – specimen width, h - specimen

thickness), a_0 - slot length, a - crack length. Correction factors [10] for specimen with hole $Y_1 = 1 - 0.1\left(\frac{2(a_0 + a)}{w}\right) + \left(\frac{2(a_0 + a)}{w}\right)^2$ and for specimen without hole $Y_2 = 1 + 0.128\left(\frac{2a}{w}\right) - 0.288\left(\frac{2a}{w}\right)^2 + 1.525\left(\frac{2a}{w}\right)^3$.

The range of short fatigue cracks (about 50 ÷ 600 μm in length) is characterized by Eq. (3) [11]. The cracks developed for the mixed mode I+II (Fig. 4b). Crack growth for a solid specimen and loading along the axis y is the sum of the crack lengths for mode I + II multiplied by cosinus of the angle plus lengths of increment of particular cracks for mode I. The crack lengths for loading in the axis x and mode I+II should be multiplied by sinus of the angle plus lengths of increment of particular cracks in this axis.

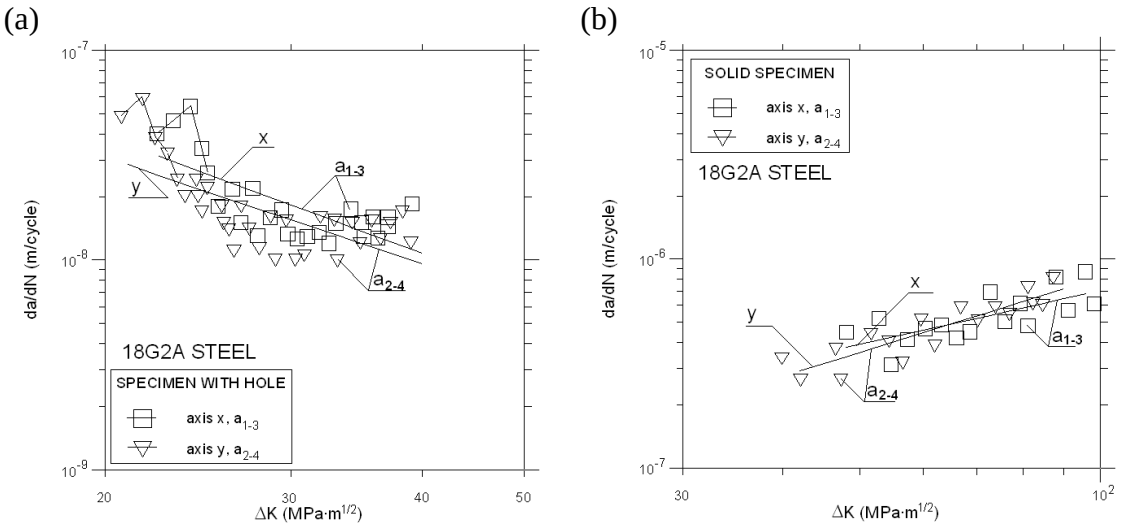

Figure 11. Comparison of the experimental results with calculated ones according to Eq. (1) for specimens: (a) with a hole, (b) without a hole

Comparing crack growth rates for the specimens with holes and without holes, we can notice that crack growth rates for the solid specimens are higher. The experimental coefficients C and m from Eq. (1) were calculated with the least square method and shown in Table 2. From Table 2 it appears that the coefficients C and m for curves x, y are different. Moreover, we can see that the coefficient of inclination of the straight line m for the specimen with the hole takes negative values, and for the solid specimen it is positive. The test results for cyclic tension-compression include a relative error not exceeding 20% (specimens with the hole not including the first three measuring points) at the 5% significance level for the correlation coefficients r given in Table 2. The coefficients of correlation in all the cases are high, so there is a significant correlation between the experimental results with the assumed model represented by Eq. (1).

Table 2. Coefficients C, m of Eq. (1) and correlation coefficients r for the curves shown in Fig. 11

Figure	C $m(MPa \cdot m^{1/2})^{-m}/cycle$	m	r
Fig. 11a, curve x	$1.005 \cdot 10^{-5}$	-1.854	-0.814
Fig. 11a, curve y	$4.688 \cdot 10^{-6}$	-1.679	-0.788
Fig. 11b, curve x	$1.371 \cdot 10^{-8}$	0.856	0.815
Fig. 11b, curve y	$3.443 \cdot 10^{-9}$	1.187	0.893

While tests, strains were measured with rosettes in order to check a degree of bending of the specimen in the points of the fatigue crack growth. From the obtained results it appears that the strain amplitude coming from bending is very low (2.6 % of the total strain) and can be neglected.

The results obtained according the analytical and numerical (FRANC3D, BES) methods were compared in Fig. 12. From Fig. 12a and 12b concerning the specimens with and without holes it appears that the values of ΔK obtained according to the analytical method are a little lower than those obtained with the numerical method under the same fatigue crack rates. Let us note that analytical results concern nominal stresses, but numerical results concern the stresses near the crack tip (Figs. 9 and 10). The authors compared the results including nominal stresses (in the numerical method about 2.5 mm from the crack front – Fig. 6). The relative error between the considered methods did not exceed 10 %.

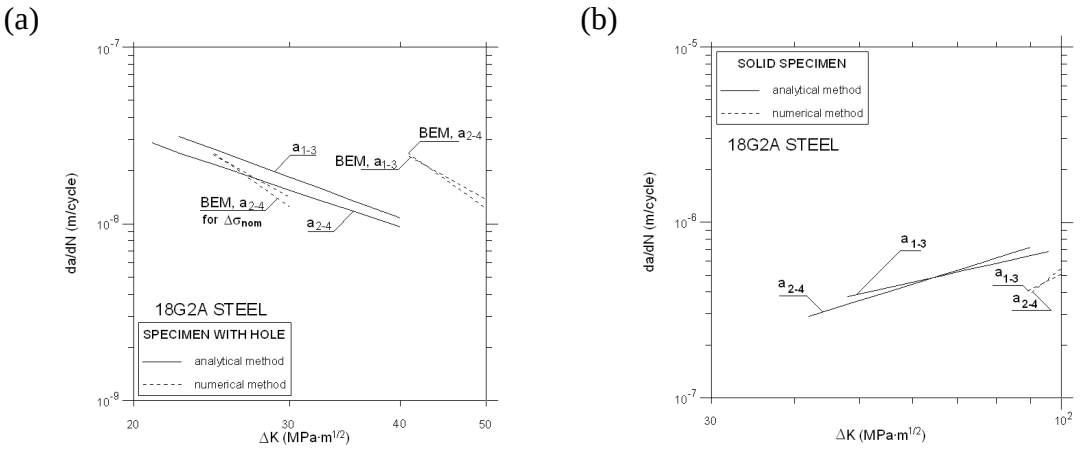

Figure 12. Comparison of the results obtained according analytical and numerical methods for specimens (a) with a hole, (b) without a hole

CONCLUSIONS

The presented results of the fatigue crack growth in the cruciform plate specimens subjected to tension-compression loading allow to formulate the following conclusions:

1. In the solid specimens, initiation and growth of the cracks occured first (to crack length about 0.6 mm) for the mixed mode I + II, next the cracks developed for mode I.
2. It has been found that the fatigue crack length in specimens with the holes the have the shapes of curves similar to logarithmic ones. In the case of solid specimens, the obtained test results form exponential curves.
3. In the case of specimens with the hole, the fatigue crack growth rate decrease, and for solid specimens, the crack growth rate increase together with increase of ΔK.
4. In the case of cruciform specimens, both analytical and numerical methods give comparable results.

REFERENCES

1. Molski, K. and Będkowski, W. (1997) Investigation of the crack growth on the cruciform specimens with sharp notches under biaxial loading, 5th Int. Conference on Biaxial/Multiaxial Fatigue and Fracture, edited by Macha E. and Mróz. Z., Technical University of Opole (Poland), 481-490.
2. Sakane, M., Ohnami, M. (1989) Creep-fatigue in biaxial stress states using cruciform specimens, Third Int. Conference on Biaxial/Multiaxial Fatigue, MPA Universitat Stuttgart, 46.1-46.18.
3. Shen, S.M. & Feng, Z.L. (1996) Fatigue crack behaviour for a corner crack at a vessel/nozzle junction, Int. J. Pres. Ves. & Piping, **68**, 319-324.
4. Rozumek, D. (2008) Fatigue crack growth rate in the cruciform specimens under proportional tension-compression, Proceedings of the 17th European Conference of Fracture (ECF17), Brno, Czech Republic, Eds. J. Pokluda et al., VUTIUM Brno, pp. 313 and CD, ps 8.
5. Thum, A., Petersen, C., Swenson, O. (1960) Verformung, Spannung und Kerbwirkung. VDI, Düesseldorf.
6. Karolczuk, A., Rozumek, D., Lachowicz, C.T., Słowik J. (2007) Initiation and growth of fatigue cracks in cruciform notched specimens, Przegląd Mechaniczny, **12**, 18-24 (in Polish).
7. COMSOL (2006), Structural Mechanics Module User's Guide, version 3.3.
8. www.cfg.cornell.edu/software/software.htm.
9. Paris, P.C., Erdogan, F. (1960) A critical analysis of crack propagation laws, J. of Basic Eng., Trans. ASME, **85**, 528-534.
10. Kocańda, S., Szala, J. (1997) Basics of Fatigue Calculations, PWN, Warsaw, (in Polish).
11. Kocańda, D., Kocańda, S., Łunarska, E., Mierzyński, J. (2005) Possibility of hydrogen-assisted propagation of short fatigue cracks in WT3-1 titanium alloy, Materials Science, **41**, 304-308.